

Numerical study on electrohydrodynamic enhancement of PCM melting in cylindrical annulus under microgravity

Kun He^a, Ben Ma^b, Lei Wang^{a,*}

^a*School of Mathematics and Physics, China University of Geosciences, Wuhan 430074, China*

^b*School of Energy and Power Engineering, Huazhong University of Science and Technology, Wuhan 430074, China*

Abstract

Latent heat thermal energy storage (LHTES) has been recommended as an effective technology to the thermal management system of space exploration for its excellent ability of storing thermal energy. However, it is well known that the low thermal conductivity of phase change material (PCM) seriously weakens the heat charging and discharging rates of LHTES system. In present study, the electrohydrodynamic (EHD), which is a popular active heat transfer enhancement technology, is introduced to enhance the PCM melting in a shell-tube LHTES system under microgravity. In our numerical simulations, we mainly focus on the combined effects of the electric Rayleigh number T and the eccentricity Γ on the melting performance under microgravity. Based on the numerical results, it is found that in contrast to the case without the electric field, the presence of the electric field causes the heat transfer efficiency and melting behavior of LHTES system to be enhanced significantly. In addition, our results indicates that the EHD technique always shows a good performance in accelerating the melting process even under microgravity, and specially, the maximum time saving in some cases is more than 90%. Furthermore, we note that although the concentric annulus is always the optimal configuration under no-gravity condition, the optimal eccentric position of the internal tube strongly depends on the electric Rayleigh number if the gravity effects are taken into account.

Keywords: Phase change, Electrohydrodynamic, Microgravity, Lattice Boltzmann method

1. Introduction

After more than a hundred years of rapid development, aerospace has become one of the most active and influential fields of science and technology in the 21st century. However, the energy supply of spacecraft in operation is time-dependent, territorial and intermittent in special space environment [1], which affects the efficient and safe operation of the spacecraft. Therefore, the need for proper thermal management system is necessary to achieve the balance between energy supply and demand, on the condition that avoids damaging the work environments of devices [2]. To ensure the security, convenience, high efficiency of energy storage and usage, the LHTES based on PCM has been recommended to some complicated aerospace system [3], and compared with the commonly sensible thermal energy

*Corresponding author

Email address: wangleir1989@126.com; leiwang@cug.edu.cn (Lei Wang)

storage and chemical energy storage methods, the distinct advantages of LHTES mainly embody in its high thermal storage density, chemical stability and small variation in temperature [4].

During the past decades, many experimental and numerical studies have been carried out to investigate the melting behavior of PCM under different gravity conditions [5, 6, 7], and these available results indicate that the LHTES technology can be served as a promising thermal energy storage method of space exploration [8]. However, since the aerospace systems is always operate under microgravity, some researchers have pointed out that the phase change heat transfer performance in this situation is seriously deteriorated as a result of the repressed attribution of nature convection [7]. Apart from this, the low thermal conductivity defect of the PCM is another unavoidable problem, which always weakens the thermal energy charging and discharging rates [9, 10]. In order to improve the heat storage efficiency of LHTES system, various heat transfer enhancement techniques have been investigated, which can be divided into two groups of passive and active heat transfer enhancement techniques [11]. The widely used passive techniques are dispersion of highly conductive nanoparticles, use of finned tubes and insertion of metal foam in the PCM [12]. In 2007, Mettawee and Assassa [13] employed dispersed micro aluminium particles to increase the conductivity of PCMs experimentally. Results show that the heat transfer rate increases with adding of aluminium mass fraction. Khodadadi and Hosseinizadeh [14] conducted a computational investigation in the same year and it was summarized that the nanoparticle-enhanced phase change materials have the higher heat release rate due to the increase of thermal conductivity and the decrease of latent heat. In addition, Lacroix and Benmadda [15] analysed the natural convection-dominated melting and solidification of PCM from a finned vertical wall, and it shows that embedding a few long fins in the PCM is more efficient for reducing the melting time than substantially augmenting the temperature of the base heated vertical wall. Wang et al. [16] numerically investigated the melting process of PCM in sleeve-tube unit with internal fins and found that the angle between neighbor fins has little impact on melting process, however, there is an optimization of the angle between neighbor fins to reduce melting time in the full-scale unit. Ruan et al. [17] explore the melting process of phase change materials in the phase change energy storage unit with fins in microgravity environment. The results show that when the phase change energy storage unit is in microgravity environment, the melting rate of the phase change material obviously decreases, and the heat is mainly transferred by the heat conduction. Moreover, Zhao et al. [18] carried out a series of phase change experiments and found that the addition of metal foam could obviously improve the overall heat transfer rate.

The aforementioned literature review shows that the passive techniques have proven to be effective at enhancing heat transfer rates in LHTES system under the ground condition or space environment, however, it is pointed out that the level of heat transfer enhancement is generally proportional to the volume of added foreign material and as the volume of added material increases, it begins to diminish the system's thermal storage density [19, 20, 21], which is usually undesirable, especially in the space environment pursuing the minimizing space. Unlike the passive techniques, the active techniques don't have these limitations and can make full use of the heat storage performance of the LHTES system. For decades, as one of the most promising active heat transfer enhancement techniques, electrohydrodynamic (EHD) has the distinct advantages of smart control, fast responding and low power consumption

[22] and has been widely applied in complex thermal energy systems (including boiling heat exchange [23], condensation heat exchange [24], and droplet evaporation [25]). Recently, in 2015, EHD technology was firstly introduced for heat transfer enhancement in LHTES systems by Nakhla et al [21]. and the experimental results showed that EHD can significantly reduce the melting time of paraffin wax. A later experiment conducted by Nakhla and Cotton [26] investigated the interaction between EHD forces and natural convection during melting of octadecane filled in a vertical latent heat thermal storage module. The results show that the use of EHD reduced the charging time by 1.7 fold, which is attributed to EHD augmenting the convection heat transfer by cell bifurcation. Quite recently, a numerical model for the EHD flow in the solid-liquid phase change process is developed by Luo et al. [27], and with this model, the electrohydrodynamic solid-liquid phase change problem was then investigated. Results show that the EHD can be a promising technique in enhancing the PCM melting, especially for the organic phase change material with low thermal conductivity and a larger latent heat term, and it is noted that the similar conclusion is also reported by Selvakumar et al. in a recent work [28].

The above mentioned works on LHTES system based on EHD are usually conducted under ground condition, however, as discussed previously, the influence of gravity is worthy of thoroughly and systematically discussion aiming at exploring efficient LHTES system for aerospace exploration. Actually, EHD enhancement technique occupies less volume compared to the passive techniques that rely on adding foreign material in the PCM. This makes EHD to be a good alternative candidate in aerospace applications, in which the space is more valuable and the aerospace system usually operate under microgravity [29, 30]. Framed in this general background, the primary task of present work is to illuminate the gravity effect on the performance of EHD to enhance the heat transfer efficiency of organic PCM inside a shell and tube unit. As far as the numerical method is concerned, the lattice Boltzmann method (LBM) is considered which has been developed into a powerful numerical solver for modeling thermal multiphase flows with phase change [31, 32, 33], as well as the EHD flows [34, 35, 36, 37]. The remainder of this paper is organized as follows. In the next section, the configuration as well as the governing equations are presented. The LBM equations are introduced in Section 3. Then, two numerical validations are carried out in Section 4 and the simulation results are discussed in detail later in Section 5. Finally, some conclusions are drawn in Section 6.

2. Physical statement and governing equations

The two-dimension physical model we considered in this paper is presented in Fig. 1. The shell-tube LHTES system filled with the solid chemical pure substance includes the inner heat transfer fluid tube with a radius of r and maintain at a constant high temperature of θ_h , and the outer cylinder shell whose radius is R keeps at a low temperature of θ_c . In order to improve the charging process in microgravity conditions, an external electric field is applied to the inner tube so that a high potential of ϕ_1 can be obtained. While the the outer shell is grounded (ϕ_0) to generate the potential difference $\phi_1 - \phi_0$, bringing in the electric-chemical reaction occurs on the surface of inner tube so homogeneous and autonomous space charge q_1 can be generated based on the charge injection model. When the

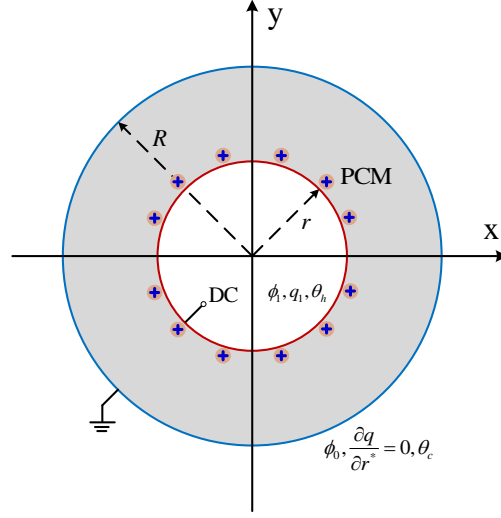


Figure 1: Schematic of phase change in a shell-tube LHTES system.

heat transfer fluid flows through the tube, heat is transferred from the hot tube to solid PCM, resulting in the melting performance and meanwhile energy is stored in the form of latent heat. In addition, due to the existence of electric field and free charges, the convection will be induced by Coulomb force with the expansion of liquid layer.

Based on the assumption of incompressible Newtonian, constant thermophysical properties fluid flow, the governing equations for phase change problem include the mass conservation Eq. 1, Navier-Stokes Eq. 2, the Gauss's law (Eq. 3), the definition of electric field (Eq. 4), the charge density conservation Eq. 5, and energy conservation Eq. 6, which can be written as:

$$\nabla \cdot \mathbf{u} = 0, \quad (1)$$

$$\frac{\partial \mathbf{u}}{\partial t} + \nabla \cdot \mathbf{u}\mathbf{u} = -\nabla p + \nabla \cdot [\nu (\nabla \mathbf{u} + (\nabla \mathbf{u})^T)] + q\mathbf{E} - \mathbf{g} [1 - \beta (\theta - \theta_r)], \quad (2)$$

$$\nabla \cdot (\varepsilon_e \nabla \phi) = -q, \quad (3)$$

$$\mathbf{E} = -\nabla \phi, \quad (4)$$

$$\frac{\partial q}{\partial t} + \nabla \cdot [q(K_e \mathbf{E} + \mathbf{u})] = \nabla \cdot (D_e \nabla q), \quad (5)$$

$$\frac{\partial H}{\partial t} + \nabla \cdot ((c_p)_e \theta \mathbf{u}) = \frac{1}{\rho_0} \nabla \cdot (\lambda_e \nabla \theta), \quad (6)$$

where $\mathbf{u} = (u_x, u_y)$ and $\mathbf{E} = (E_x, E_y)$ are fluid velocity field and electric field, respectively. The scalars $p, \nu, q, \beta, \theta, \phi, H, \rho_0$ represent for the pressure, kinematic viscosity, charge density, volumetric expansion coefficient, temperature, electric potential, total enthalpy and fluid density. In addition, the symbols $\varepsilon_e, K_e, D_e, (c_p)_e, \lambda_e$ are electrical permittivity, ionic mobility, charge diffusion coefficient, specific heat and thermal conductivity. Among them, the subscript

e stands for efficient parameters, which means the values of those parameters for solid and liquid phase are different. Moreover, Eq. 6 is the total enthalpy-based energy conservation equation, and the definition of H is given as:

$$H = c_p\theta + f_l L, \quad (7)$$

where f_l , L are the liquid fraction and latent heat of PCM, respectively. Obviously, the total enthalpy can be divided into two parts, the sensible heat $C_p\theta$ and latent heat $f_l L$. Then, the melting process is governed by the following seven dimensionless parameters:

$$\begin{aligned} Ra &= \frac{g\beta(\theta_h - \theta_c)L^3}{\nu\chi}, & T &= \frac{\varepsilon(\phi_1 - \phi_0)}{\mu K}, & C &= \frac{q_1 l^2}{\varepsilon(\phi_1 - \phi_0)}, \\ M &= \frac{1}{K} \left(\frac{\varepsilon}{\rho}\right)^{1/2}, & Pr &= \frac{\nu(\rho c_p)}{\lambda}, & \alpha &= \frac{D}{K(\phi_1 - \phi_0)}, & Ste &= \frac{C_p \Delta T}{L}. \end{aligned} \quad (8)$$

Ra , defined as the ratio between the buoyancy and viscous force, is the Rayleigh number, indicating the strengthen of gravity effect. Similar with Ra , the electric Rayleigh number T , which is the ratio of Coulomb force and viscous force, measures the intensity of Coulomb force. C and α is the charge injection strength and charge diffusion coefficient. The other three parameters represent for the physical properties of fluids. Prandtl number Pr is defined as the ratio of momentum diffusion capacity to heat diffusion capacity. Further, M is the non-dimensional mobility. The Stefan number Ste indicates the ratio of sensible and latent heat of PCM. Additionally, the maximum magnitude of velocity and dimensionless time Fourier number are adopted to measure the flow motion and melting process for phase change problem, which are defined as:

$$V_{max} = \max(\sqrt{u^2 + v^2}), \quad Fo = \frac{\lambda t}{(\rho c_p) l^2}, \quad (9)$$

3. The lattice Boltzmann equations

3.1. Lattice Boltzmann equation for flow field

In this work, the incompressible lattice Bhatnagar-Gross-Krook (LBGK) proposed by Guo et al. [38] is adopted to simulate the fluid field, and the evolution of the particle velocity distribution function reads:

$$f_i(\mathbf{x} + \mathbf{c}_i \Delta t, t + \Delta t) - f_i(\mathbf{x}, t) = -\frac{1}{\tau_l} [f_i(\mathbf{x}, t) - f_i^{(eq)}(\mathbf{x}, t)] + \Delta t F_i, \quad (10)$$

where \mathbf{c}_i , Δt are the discrete velocity and time step, respectively. τ_l is the dimensionless relaxation time, depending on the fluid viscosity as a function of $\nu = \rho_0 c_s^2 (\tau_l - 0.5) \Delta t$. In addition, the $f_i(\mathbf{x}, t)$ is the distribution function at time t and location \mathbf{x} in direction i . Further, the local equilibrium distribution function $f_i^{(eq)}(\mathbf{x}, t)$ is defined as:

$$f_i^{(eq)}(\mathbf{x}, t) = \eta_i p + \omega_i \left[\frac{\mathbf{c}_i \cdot \mathbf{u}}{c_s^2} + \frac{\mathbf{u} \mathbf{u} : (\mathbf{c}_i \mathbf{c}_i - c_s^2 \mathbf{I})}{2c_s^4} \right], \quad (11)$$

where \mathbf{I} is the two second-order identity matrix. w_i and \mathbf{c}_i are weight coefficient and discrete velocity in the direction of i , which depends on the DnQq (n-dimensional q-velocity) model we used. For all evolution functions except for

the electric field, the classical D2Q9 discrete velocity model proposed by Qian et al. [39] is considered, and the w_i and \mathbf{c}_i are given by:

$$\omega_i = \begin{cases} 4/9, & i = 0, \\ 1/9, & i = 1 - 4, \\ 1/36, & i = 5 - 8, \end{cases} \quad (12)$$

$$\mathbf{c}_i = \begin{cases} (0, 0), & i = 0, \\ c \left(\cos \left[(i-1) \frac{\pi}{2} \right], \sin \left[(i-1) \frac{\pi}{2} \right] \right), & i = 1 - 4, \\ \sqrt{2}c \left(\cos \left[(2i-1) \frac{\pi}{4} \right], \sin \left[(2i-1) \frac{\pi}{4} \right] \right), & i = 5 - 8. \end{cases} \quad (13)$$

where $c = \Delta x / \Delta t$ is the streaming speed, and related to the sound speed through $c_s = c / \sqrt{3}$. Among them, Δx is the lattice space. In addition, η_i is the model parameter, calculating by $\eta_0 = (\omega_0 - 1) / c_s^2 + \rho_0$, $\eta_i = \omega_i / c_s^2 (i \neq 0)$ with ρ_0 being the average density. Moreover, an external force term needs to be added in Eq. 10 to exert the influence of buoyancy and Coulomb force on flow motion. Based on the the modified second-order moment model proposed by Guo et al. [40], the force term can be expressed as:

$$F_i(\mathbf{x}, t) = \omega_i \left(1 - \frac{1}{2\tau_f} \right) \left[\frac{\mathbf{c}_i \cdot \mathbf{F}}{c_s^2} + \frac{(\mathbf{F}\mathbf{u} + \mathbf{u}\mathbf{F}) : (\mathbf{c}_i \mathbf{c}_i - c_s^2 \mathbf{I})}{2c_s^4} \right], \quad (14)$$

where $F = q\mathbf{E} + \mathbf{g}\beta_l(\theta - \theta_0)$. Then, the macroscopic qualities including the velocity field and pressure can be evaluated by:

$$\mathbf{u} = \sum_i \mathbf{c}_i f_i + \frac{\Delta t}{2} \mathbf{F}, \quad (15)$$

$$p = \frac{c_s^2}{1 - \omega_0} \left(\sum_{i \neq 0} f_i - \omega_0 \frac{|\mathbf{u}|^2}{2c_s^2} \right). \quad (16)$$

3.2. Lattice Boltzmann equation for electric potential

Unlike the standard convection-diffusion equation, the Poisson equation which governs both the solid and liquid phase is essential a steady state equation. In order to accurately solve the Poisson equation, an improved LB model developed by Chai et al. [41] is applied, and the evolution function for electric potential reads:

$$g_i(\mathbf{x} + \mathbf{c}_i \Delta t, t + \Delta t) - g_i(\mathbf{x}, t) = -\frac{1}{\tau_\phi} \left[g_i(\mathbf{x}, t) - g_i^{(eq)}(\mathbf{x}, t) \right] + \Delta t \hat{\omega}_i \xi \varepsilon_i R, \quad (17)$$

where ξ is the artificial model coefficient, controlling the evolution speed of electric potential. In addition, the source term R is defined as $R = q / \varepsilon_e$, in which ε_e equals ε_l for liquid region, while equals ε_s for solid region. Moreover, ε_i represents the ratio between ε_e and ε_l . Further, the D2Q5 discrete scheme is considered and the local equilibrium distribution function $g_i^{(eq)}(\mathbf{x}, t)$ reads:

$$g_i^{(eq)} = \begin{cases} (\hat{\omega}_0 - 1) \phi, & i = 0, \\ \hat{\omega}_i \phi, & i = 1 - 4. \end{cases} \quad (18)$$

In this model, the weight coefficient $\hat{\omega}$ is given by:

$$\hat{\omega}_i = \begin{cases} 0, & i = 0, \\ 1/4, & i = 1 - 4, \end{cases} \quad (19)$$

where $\hat{c}_s^2 = c^2/2$. The relaxation time τ_ϕ for potential relays on the coefficient ξ and ε_t through $\xi\varepsilon_t = \hat{c}_s^2(\tau_\phi - 0.5)\Delta t$. Further, the electrical potential is calculated by:

$$\phi = \frac{1}{1 - \omega_0} \sum_i g_i. \quad (20)$$

In addition, the whole electric field distribution must be determined in order to couple the electric field and flow field by Coulomb force. The most straightforward method is to apply the difference scheme to the definition of electric field (Eq. 5). However, due to the kinetic essence of the LBM, \mathbf{E} can be evaluated locally by:

$$\mathbf{E} = \frac{1}{\tau_\phi \hat{c}_s^2} \sum_i \mathbf{c}_i g_i. \quad (21)$$

3.3. Lattice Boltzmann equation for charge density

Charge transport equation solving is the pivotal part in EHD problems owing to the strong convection-dominating characteristic. Following the works of Luo et al., [27] the evolution equation for charge density is expressed as:

$$h_i(\mathbf{x} + \mathbf{c}_i \Delta t, t + \Delta t) - h_i(\mathbf{x}, t) = -\frac{1}{\tau_q} [h_i(\mathbf{x}, t) - h_i^{(eq)}(\mathbf{x}, t)], \quad (22)$$

where τ_q is the non-dimension relaxation time for charge density, and depends on the charge diffusion coefficient D_e as a function of:

$$D_e = c_s^2(\tau_q - 0.5)\Delta t. \quad (23)$$

Therefore, it equals $\alpha(\phi_1 - \phi_0)K_l$, $\alpha(\phi_1 - \phi_0)K_s$ for liquid phase and solid phase, respectively. Moreover, the local equilibrium equation function $h_i^{(eq)}(\mathbf{x}, t)$ is defined as:

$$h_i^{(eq)}(\mathbf{x}, t) = q\omega_i \left\{ 1 + \frac{\mathbf{c}_i \cdot (K_e \mathbf{E} + \mathbf{u})}{c_s^2} + \frac{[\mathbf{c}_i \cdot (K_e \mathbf{E} + \mathbf{u})]^2 - c_s^2 |K_e \mathbf{E} + \mathbf{u}|^2}{2c_s^4} \right\}. \quad (24)$$

Further, the macroscopic charge density is obtained by:

$$q = \sum_i h_i. \quad (25)$$

3.4. Lattice Boltzmann equation for temperature field

The simple boundary treatment for phase interface makes the LBM convenient to deal with the phase change problems and several LB models have been proposed [42, 31]. However, the unphysical numerical diffusion across the phase interface indicates that those models may be not accurately track the phase change interface. Recently, a newly developed optimal two-relaxation-time (OTRT) lattice Boltzmann model, based on the Chapman-Enskog expansion,

shows the great efficiency in eliminating the unphysical numerical diffusion for arbitrary discrete velocity model [43]. To this end, the OTRT model is employed here to solve the energy conservation equation, and the evolution function can be expressed as:

$$l_i(\mathbf{x} + \mathbf{c}_i \Delta t, t + \Delta t) = l_i^{(eq)}(\mathbf{x}, t) + \left(1 - \frac{1}{2\tau_s} - \frac{1}{2\tau_a}\right) [l_i(\mathbf{x}, t) - l_i^{(eq)}(\mathbf{x}, t)] - \left(\frac{1}{2\tau_s} - \frac{1}{2\tau_a}\right) [l_i(\mathbf{x}, t) - l_i^{(eq)}(\mathbf{x}, t)], \quad (26)$$

where τ_s and τ_a denote the symmetric and anti-symmetric relaxation time. l_i and $l_i^{(eq)}$ represent the distribution function and equilibrium distribution function along the opposite direction, respectively. Among them, the local equilibrium distribution function are defined as:

$$l_i^{eq} = \begin{cases} H - c_p \theta + \omega_i c_p \theta \left(1 - \frac{|\mathbf{u}|^2}{2c_s^2}\right), & i = 0, \\ \omega_i c_p \theta \left[1 + \frac{\mathbf{c}_i \cdot \mathbf{u}}{c_s^2} + \frac{(\mathbf{c}_i \cdot \mathbf{u})^2}{2c_s^4} - \frac{|\mathbf{u}|^2}{2c_s^2}\right], & i \neq 0. \end{cases} \quad (27)$$

In this context, the anti-symmetric relaxation time is calculated by:

$$\frac{\lambda}{\rho_0 c_p} = c_s^2 (\tau_a - 0.5) \Delta t, \quad (28)$$

and the symmetric relaxation time can be evaluated from

$$\frac{1}{\tau_s} + \frac{1}{\tau_a} = 2. \quad (29)$$

Then, the total enthalpy can be obtained by:

$$H = \sum_i l_i. \quad (30)$$

Once H is determined, the total liquid fraction f_l and temperature θ can be also calculated through the following thermodynamic relations:

$$f_l = \begin{cases} 0 & H \leq H_s \\ \frac{H - H_s}{H_l - H_s} & H_s < H < H_l \\ 1 & H \geq H_l \end{cases} \quad (31)$$

$$\theta = \begin{cases} \frac{H}{c_p} & H \leq H_s \\ \frac{H_l - H}{H_l - H_s} \theta_s + \frac{H - H_s}{H_l - H_s} \theta_l & H_s < H < H_l \\ \theta_l + \frac{H - H_l}{c_p} & H \geq H_l \end{cases} \quad (32)$$

in which H_s and H_l are the total enthalpy at solidus temperature θ_s and liquidus temperature θ_l , respectively. In this work, two-dimensional one-phase melting is considered ($\theta_s = \theta_l = \theta_m$).

4. Code verification

In this section, two validations tests are performed to verify the accuracy of the present LB model. Firstly, we consider the melting of PCM inside a square cavity, and the evolution of total liquid fraction and average Nusselt number during the melting process are presented in Fig. 2(a) and Fig. 2(b), from which we can see that the present results

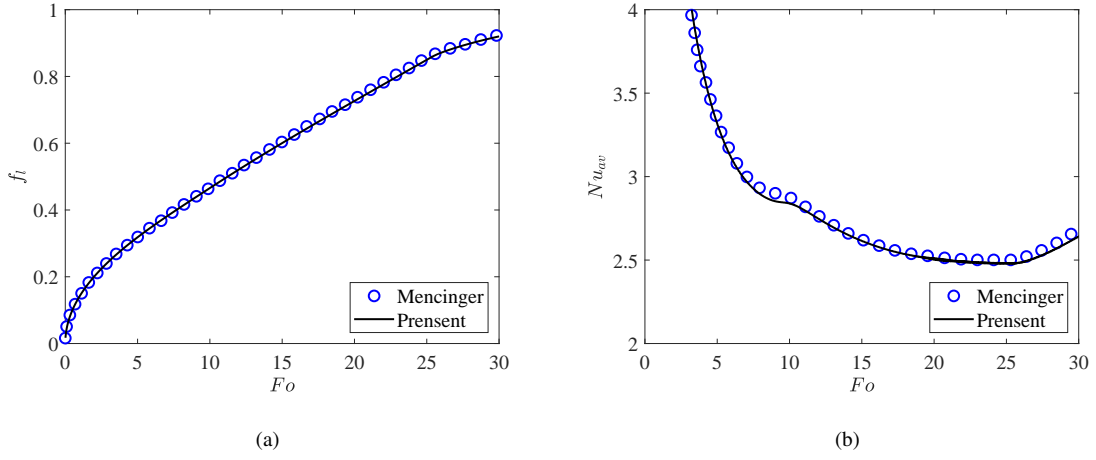


Figure 2: The comparisons of (a) total liquid fraction and (b) average Nusselt number with Fo between present numerical results and Mencinger's [44] results.

agree well with the benchmark solutions reported in Ref [44]. Further, in the second test, the analytic hydrostatic solutions between two concentric cylinders are compared with our present numerical results. The analytical solution of hydrostatic state can be found in Ref. [45]. As shown in Fig. 3(a) and Fig. 3(b), the profiles of charge density and the electric field strength in the radial direction obtained from our numerical results show good agreements with the analytical solutions. In addition, Fig. 4 shows the evolution of total liquid fraction for three different grid resolutions (320×320 , 512×512 , 800×800) for the case of $T = 2500$, $\Gamma = 0.0$ under the gravity condition of $1g$, and it can be found that the grid resolution of 512×512 can give to the grid independence results.

5. Results and discussions

In this section, EHD melting performance of organic dielectric PCM filled in a cylindrical annulus LHTES system under microgravity conditions is systematically investigated. The numerical results are presented for the instantaneous distributions of charge density, temperature and flow fields, as well as the liquid-solid interface in charging process. Moreover, the total melting time is also considered to compare the melting performance improvement. If no special instructions, all the computations are performed under the strong charge injection with $C = 10$ and the dimensionless charge diffusion number with $\alpha = 10^{-3}$, while the non-dimensional mobility parameter (M), Prandtl number (Pr) and Stefan number (Ste) are fixed at 40, 30 and 0.1, respectively, which are in the range of typically organic dielectric PCMs used in LHTES [28]. Additionally, the ratios of dielectric permittivity and ionic mobility between the liquid and the solid phases are set to be 2.0. Further, in order to reveal the effects of the external electric field, the impacts of EHD on phase change heat transfer performance under no-gravity condition are first evaluated. Moreover, the effect of electric Rayleigh number (T), gravitational accelerations and eccentricity (Γ) are also presented and discussed.

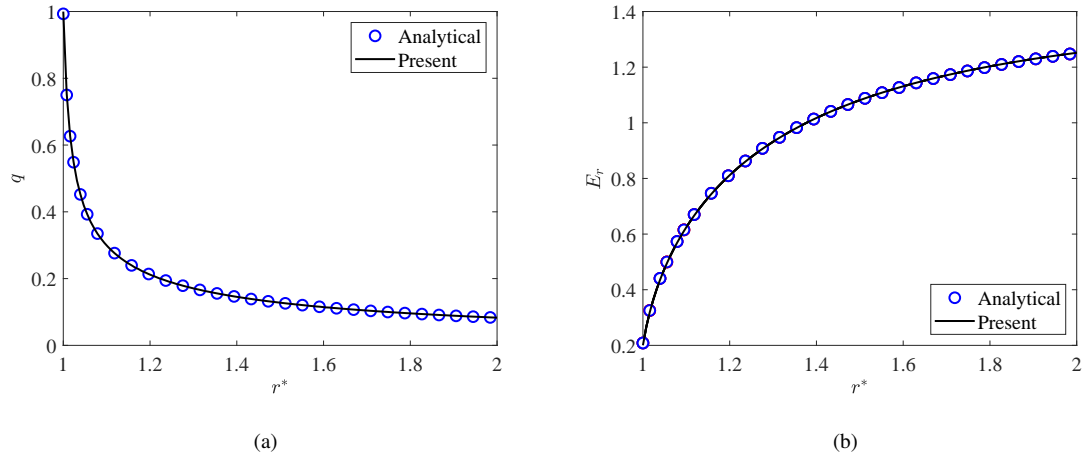


Figure 3: The comparisons of (a) charge density and (b) electric field strength at hydrostatic state between present numerical results and analytical solutions.

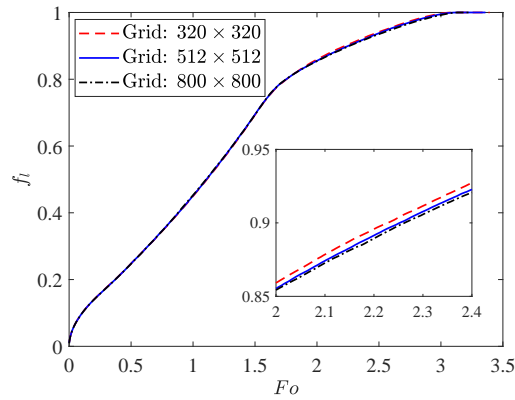


Figure 4: The grid independence test.

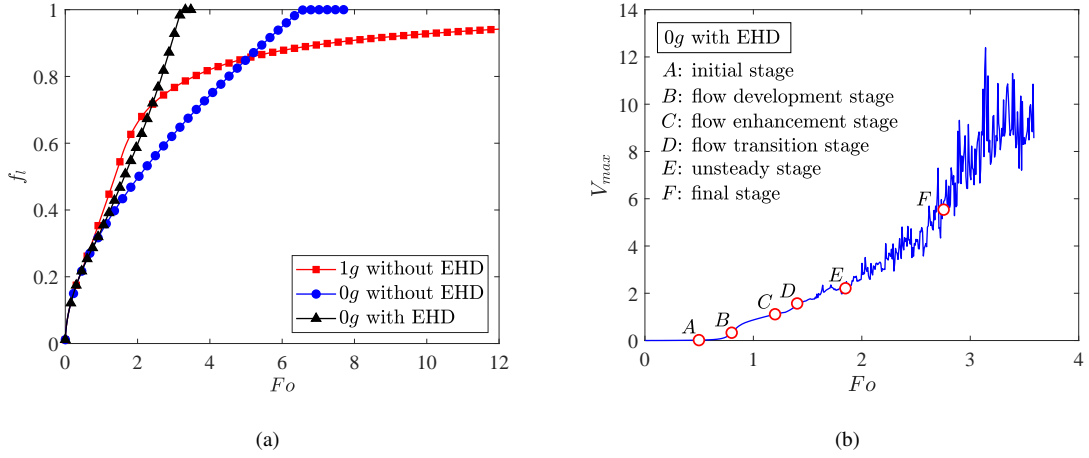


Figure 5: Time evolution process of (a) the total liquid fraction f_l and (b) the maximum flow velocity V_{max} .

5.1. The transient charging process of PCM under no-gravity condition

In order to have a preliminary insight into the charging process of PCM with an external electric field under no-gravity condition (0g), time evolution process of the total liquid fraction f_l at $T = 1000$ is presented in Fig. 5(a), in which the cases of normal gravity (1g) and no-gravity conditions (0g) without electric field are also incorporated as a comparison. An overview indicates that the LHTES system with an external electric field and charge injection consumes the shortest time for PCM to completely melt. More specifically, both the above share the similar evolution of liquid fraction at the early stage of melting when heat is mainly transported by conduction mode. Meanwhile, a higher melting rate can be obtained due to the relatively large temperature gradient between a thin liquid layer. As melting continues, the PCM under normal gravity is the first to melt at a higher rate as a result of the vortex circulation in the melted PCM caused by buoyancy, but the melting process will be slowed down after the upper half of the melting is completed due to the heat accumulation in the upper region [33]. Unlike that, heat can be symmetrically conducted into the surrounding solids in all directions for the case of no-gravity conditions. However, the thermal resistance will increase as the liquid layer thickens, resulting in a continuous decrease in the melting rate. After applying the electric field, as shown in Fig. 5(a), the melting always proceeds at a higher speed with the existence of Coulomb-driven convection, and compared to the case of no-gravity conditions, a time saving of 54% is obtained.

To better understand the whole evolution process from the solid phase to complete liquid phase, Fig. 5(b) plots the corresponding time evolution of maximum flow velocity V_{max} . It is conveniently to approximately divide the whole charging process into six stages marked as points A, B, C, D, E and F, respectively. The corresponding distributions of charge density, temperature field and the liquid fraction with streamlines are shown in Fig. 6. It can be clearly seen that in the initial stage, a thin liquid layer is formed symmetrically around the hot inner cylindrical electrode and no flow motion can be observed due to the uniform charge density distribution which leads to the weak Coulomb force. At this time, free charges can transport only by the drift and diffusion mechanisms, and conduction is the

main mode of heat transfer in the melting process. As melting continues, the Coulomb force gradually increases and finally overcomes the viscous force, resulting in the induction of a radial motion with sixteen pairs of counter-rotating vortices at $Fo = 0.80$. In this way, the isotherm begins to deform on the account of the enhancement of convective heat transfer. Along with the increasing of flow intensity, electric convection is fully developed at point C , featured by the formation of charge void region around the cylindrical electrode. Then, under the influence of radial flow, sixteen thermal plumes can be clearly observed, which evenly distribute around the inner cylinder and impinge toward the outer cylinder. At this moment, heat is transferred as a passive scalar to the solid-liquid interface, which takes the shape of petal around the heat source. With the further development of melting, vortices merged in pairs resulting in a transition happens from a sixteen pairs of vortices pattern to a twelve pairs of vortices pattern. The reason for this is attributed to the most unstable mode of the electric convection system determined by stability analysis [46]. Afterwards, accompanied by some vortices generating and vanishing, the flow bifurcates into the unsteady state and the solid-liquid interface is smoothed as a result of irregular flow motion and heat transfer. Finally, due to the strong nonlinear instabilities, electric and thermal plumes are generated randomly and intermittently. This type of plumes turn the shape of solid-liquid interface into a circle circular in the final stage and it can be concluded that under no-gravity condition, all parts of the PCM melt almost simultaneously under the influence of electroconvection induced by the electric field.

5.2. Effect of electric Rayleigh number T on the charging process

Based on above discussion, the charging efficiency of the LHTES system under no-gravity condition can be effectively improved by employing an electric field and unipolar charge injection. It is well-known that the electroconvection induced by Coulomb force greatly depends on the electric Rayleigh number T . Therefore, it is necessary to investigate the melting performance improvement by considering the influence of the electric Rayleigh number T . In this section, the melting process of LHTES devices with different T under no-gravity condition is presented and discussed. In order to quantitatively reflect the enhancement of melting performance, an evaluation factor Φ is defined to calculate the percentage of charging time reduction when electric field is applied compared with no EHD effect, expressed as:

$$\Phi = \frac{t_0 - t_1}{t_0} \times 100\%, \quad (33)$$

in which t_0 and t_1 represent the time consumption for the cases without and with EHD technology, respectively.

Fig. 7 presents the variation of total liquid fraction f_l with melting time and the percentages of charging time reduction for various electric Rayleigh number T , in which the label $T = 0$ indicates the case of melting without electric field. Apparently, a higher electric driving parameter T can give rise to a shorter charging time of the system. However, when T exceeds 1500, the effect is not immediately significant. Therefore, a T higher than 1500 is not recommended from the perspective of energy consumption. Moreover, after the initial melting stage dominated by conduction, the increase rate of total liquid fraction expressed by the slope of curve is positively related to electric Rayleigh number, and several "separation points" can be observed from these curves, which directly reflect the

influence of EHD on melting. In fact, for a larger electric Rayleigh number, the earlier electroconvection can be motivated by the stronger electric field, which corresponds to an earlier separation point. To illustrate this, distributions of charge density, temperature field and the liquid fraction with streamlines at four representative time for $T = 2500$ are presented in Fig. 8, which can be compared with the case of $T = 1000$ in Fig. 6. It can be seen that after a short initial period of conduction-dominated melting, electroconvection with twenty-eight pairs of counter-rotating vortices are rapidly formed at $Fo = 0.35$, while for the case of $T = 1000$, the flow motion has not yet begun at this moment. Additionally, the number of vortices for $T = 2500$ is almost twice than it of $T = 1000$, and the increase in convective cell number is conducive for heat transfer in the liquid layer. Subsequently, with the merging of vortices, unstable flow motion is formed, which eventually develops into a chaotic state, leading to the rapid completion of melting. Quantitatively, compared with the case of pure-conduction melting under on-gravity condition, a time saving of about 34%, 54%, 64%, 69%, 73% can be obtained for $T = 500$, $T = 1000$, $T = 1500$, $T = 2000$, and $T = 2500$, respectively, as shown in Fig. 7(b).

5.3. Effect of gravity conditions on the charging process

It is well-known that the space environment is always microgravity or even no-gravity. Therefore, investigations on melting process under different gravity conditions are essential. In this section, the performance of EHD to enhance heat transfer during melting process under six gravity environments (0g, 0.1g, 0.3g, 0.5g, 0.8g, 1g) is considered. Fig. 9(a) depicts the influence of electric Rayleigh number on total melting time under different gravity conditions. It can be clearly seen from Fig. 9(a) that EHD technology plays an important role in improving the overall energy storage efficiency of LHTES system. In general, the electro-thermo-convection in LHTES systems would be strengthened with the increase of T , and thereby reducing the total melting time. Actually, almost all of the cases considered follow this rule except for the situation that the gravity effect is quite great and a weak Coulomb force cannot balance the buoyancy, leading to the worse melting efficiency. As a result, there exists a maximum for total melting time at $T = 500$, which is quite different compared with other gravity conditions. The reason for this phenomenon is attributed to the radial Coulomb force, which intensifies the accumulation of heat in the upper region. In order to have an intuitive interpretation, the profiles of temperature along the horizontal central line of the lower region at a representative time of $Fo = 30$ in the melting process for $T = 0$ and $T = 500$ are depicted in Fig. 9(b), in which the corresponding temperature distributions are also incorporated. It can be found that once the electric field is applied, the temperature in this part is lower than that of no electric field, indicating less heat can be observed by the non-melted PCM in the bottom section. Actually, since Coulomb force is too weak to stimulate the electroconvection in this case, buoyancy dominates the melting process, and both heat and ions tend to accumulate upward, resulting in a slow melting rate in the lower part. Moreover, when the electric Rayleigh number is sufficiently high, i.e. $T \geq 1500$, it is uneconomical to improve the heat transfer efficiency by increasing T , as the almost horizontal curves in Fig. 9(a).

Fig. 9(a) also proves that the gravity effect has a significant impact on the melting time, especially for a small T . Nevertheless, the influence of gravity effect on total melting time is almost negligible when T is sufficiently high, and

in this case, the Coulomb-driven electroconvection plays a leading role in heat transfer during the melting process. For intuitive understanding of the melting process and comparisons between various gravity conditions, distributions of charge density, temperature and solid-liquid interface with streamlines for $T = 1500$ at $Fo = 1.0$ are shown in Fig. 10. An overview indicates that the existence of gravity has significant influence on melting behaviors due to the comprehensive combinations of upward buoyancy and radical Coulomb force. More specifically, for a large value of gravity, i.e., $1.0g, 0.5g$, the charge void regions merely appear at upper half of the system, indicating the convection is fairly strong and heat is gathered in those areas. This can be explained by that the buoyancy together with the Coulomb force act on the similar direction, contributing for the increase of flow intensity and heat transfer enhancement. As a result, the interface and vortices are quite irregular at the upper part, while for the lower part, the smooth interface and streamlines means that melting mainly depends on heat conduction. Therefore, the liquid phase layer is relatively thinner. When the gravity is further decreased to $0.3g$, the contributions for melting made by buoyancy are greatly weakened and heat can be transported to the lower part by the radial Coulomb force. As a result, flow motion has been enhanced with the formation of charge void regions, which are smaller compared to it in the upper part. In addition, the whole convective cells also fall off into secondary eddies leads to the petal shaped interface. As far as the case of $0g$, the buoyancy is completely ignored. The charge void regions which are distributed uniformly around the inner cylinder can be clearly seen and the petal shaped interface are more obvious.

Quantitatively, the charging time under different gravity conditions as well as the corresponding evaluation factor is summarized in Table. 1 and conclusion can be drawn that EHD technology has an excellent performance in improving the melting efficiency of PCM and shortening the heat storage time of the LHTES system under microgravity condition. Specifically, the melting time can be saved by up to 95% with EHD, and a melting time saving of 76% can be also obtained for the case of no-gravity condition, which indicates that EHD can be a favorable candidate for enhancing the heat storage efficiency of LHTES system in aerospace.

Table 1: Charging time under different gravity conditions.

Gravity condition	0g	0.1g	0.3g	0.5g	0.8g	1g
Total melting time without EHD (t_0)	7.79	30.94	42.75	46.00	48.05	49.90
Total melting time with EHD (t_1)	2.10	2.14	2.23	2.61	3.00	3.30
The percentage of charging time reduction (Φ)	73%	93%	95%	94%	94%	93%

5.4. Effect of eccentricity on the charging process

Some previous research results have shown that the location of internal cylindrical tube of the LHTES system has an important influence on the charging process of PCM without EHD, and an eccentric design has been an attractive configuration optimization method, which can accelerate the melting of PCM by making full use of natural convection [47, 48, 49]. Based on this foundation, we now turn to study the influence of eccentricity Γ on melting process of PCM

with the existence of electric field, and the eccentricity is defined as $\Gamma = l_0/(R - r)$, where l_0 is the centre-to-centre distances [50]. Additionally, taking into account the radial direction of electric field and the upward buoyancy, we only consider the case where the internal tube is placed downward in present study. For the one hand, the bottom of the system is the pivotal regions that melting is fairly slower. For the other hand, it is convenient to better understand the synergy between the electric field and the gravity effect.

Fig. 11 depicts the influence of eccentricity on total melting time under no-gravity condition, in which the effect of electric Rayleigh number is also involved. It can be obviously seen that the total melting time increases with the increase of eccentricity, which indicates that the charging time of LHTES system is prolonged by moving downward the internal tube. Therefore, the eccentric cylindrical configuration is not feasible for melting with EHD under no-gravity condition. This is easy to understand: since the direction of electric field is radial, a centrally placed tube is more conducive to develop the symmetrical convection, which can transfer heat uniformly to all directions of PCM. For further insight into the influence of eccentricity on the melting process of PCM under the action of electric field, distributions of charge density, temperature and the total liquid fraction with streamlines for $T = 1000$ at $Fo = 1.2$ are presented in Fig. 12. Obviously, the position of internal tube has a significant impact on the melting behaviors as a result of the inhomogeneous distributions of charge density and electric field. More specifically, compared with the case of centrally placed tube [see Fig. 6], the area of charge void regions tends to shrink and the electric plumes become much thinner in the lower part when the inner tube is moved slightly downward, i.e., $\Gamma = 0.095$. At the same time, more eddies are formed in the lower area, so higher heat transfer efficiency can be obtained due to the increase in flow strength, resulting in a more curly solid-liquid interface in this region. As eccentricity is further increased to $\Gamma = 0.261$, an interesting phenomenon occurs that the upper and lower half of the solid-liquid interface become smooth, and it needs to be pointed that the reasons for the smoothness of the two parts are quite different. In the lower part, flow becomes unstable due to a larger voltage drop caused by the eccentric cylindrical settings. Consequently, more melted PCM can be observed in this part and the interface turns to be smooth because of the swing of electric plumes, while in the upper part, the intensity of electroconvection is weakened by the decrease of Coulomb driving force due to the farther distance from the electrode, and the heat transfer efficiency decreases accompanied with the thickening of the thermal layer boundary. For a large value of eccentricity, i.e., $\Gamma = 0.400$, $\Gamma = 0.519$, the Coulomb force is too small to sustain the flow motion in the upper region, and then both the charge void region and vortex disappear leading to a slow conduction-dominated melting process, featured by a uniform temperature distribution. Conversely, flow bifurcates into the chaotic state and most of the PCM has melted in the lower region due to the quite strong convection. That is why the melting process is slowed when employed a eccentric cylindrical configuration: the balance of the symmetrical electric field is broken, leading to the concentration of charge and heat in the lower part of the system.

On this basis, we further explore the melting efficiency of the eccentric cylindrical LHTES system under the combined influence of Coulomb and buoyancy force. The effect of eccentricity on total melting time under normal gravity condition is presented in Fig. 11(b), from which can be seen that when T is small, i.e., $T = 1000$, the

total melting time decreases with the increase of Γ . At this time, the upward buoyancy plays more important role in melting process. While for larger T , i.e., $T \geq 1500$, as shown in Fig. 11(b), a critical value for a given electric Rayleigh number can be observed, which corresponds to the minimum time consuming. Besides, it is interesting to point out that as T increases, the optimal position gradually moves up, approaching the center of the outer cylinder shell. The main reason for the variation is the fact that the synergistic effect between the upward buoyancy and the radial Coulomb force. In the upper region, the two driving forces act on a similar direction and jointly promote the melting of PCM. While in the lower half, the electroconvection induced by the Coulomb one can still provide a high heat transfer rate and contribute the PCM in this area to melt, which is not available in the melting process dominated by buoyancy. Quantitatively, the minimum time consuming is 3.33, 2.69, 2.59 for $T = 1500$, $T = 2000$ and $T = 2500$, respectively. Compared to the case of concentric annuli, a maximum time saving of about 60%, 42%, 21% can be obtained by moving downward the internal tube.

6. Conclusions

In this paper, the effect of electric field on melting of PCM in cylindrical annulus under microgravity conditions is investigated by LBM. Four different evolution equations are employed to reveal the complex phase change characteristics of the LHTES system. In addition, due to the intrinsic parallelism nature of LBM, all simulations conducted in this work are implemented on the Graphics Processor Units (GPUs) using NVIDIA's CUDA for a high computation efficiency. According to the present simulation results, some major conclusions are summarized as following:

(1) Under no-gravity condition, the melting rate can be significantly improved by applying an external electric field and unipolar charge injection. Due to heat can be uniformly transferred along with radial direction of heat source, all parts of the PCM melt almost simultaneously under the influence of strong electroconvection induced by Coulomb force.

(2) Increasing the driving force T greatly shortened the complete charging time for LHTES system, and a maximum time saving of 95% can be obtained under the gravity condition of 0.3g for $T = 2500$.

(3) Gravity effect has a considerable impact on the total melting time by adjusting the effect of buoyancy for a small value of T . While it can be almost negligible when T is sufficiently large to dominate the convection with the increase of liquid phase.

(4) Under the condition of no-gravity, the LHTES device with concentric annuli configuration obtains the best melting performance compared with the eccentric cylindrical cases. When considering the effect of gravity, the optimal location of the heated electrode depends on the comprehensive results of the buoyancy and Coulomb force and a maximum time saving of 60% can be obtained by employing an eccentric cylindrical configuration compared with the concentric annuli case.

Based on the above results, conclusions can be drawn that the radial electroconvection plays an important role in improving the heat transfer efficiency during melting process under microgravity conditions, and it can be regarded as a

good supplement for heat transfer enhancement, since the attribution of natural convection on heat transfer is repressed due to the weakened buoyancy in this situation. From the great performance of EHD technology in the microgravity environment, it is believed that EHD can be a favorable candidate for enhancing the heat storage efficiency of LHTES system in aerospace.

Acknowledgments

This work was financially supported by the National Natural Science Foundation of China (No. 12002320), and the Fundamental Research Funds for the Central Universities (No. CUG180618 and CUGGC05).

Conflicts of interest

The authors declare no conflict of interest.

References

- [1] Li X, Zhu Z, Xu Z, Ma T, Zhang H, Liu J, Wang Q. Effect of supergravity on heat transfer characteristics of PCM with the pore-scale lattice Boltzmann method. *Energy Procedia* 2019;158:4641-47.
- [2] Li X, Ma T, Liu J, Zhang H, Wang Q. Pore-scale investigation of gravity effects on phase change heat transfer characteristics using lattice Boltzmann method. *Appl Energy* 2018;222:92-103.
- [3] Li X, Zhu Z, Xu Z, Ma T, Zhang H, Liu J, Wang X, Wang Q. A three-dimensional pore-scale lattice Boltzmann model for investigating the supergravity effects on charging process. *Appl Energy* 2019;254:113507.
- [4] Farid MM, Khudhair AM, Razack SAK, Al-Hallaj S. A review on phase change energy storage: materials and applications. *Energy Convers Manage* 2004;45:1597-615.
- [5] Tolbert C. Experimental results from the thermal energy storage-2 (TES-2) flight experiment. NASA/TM-2000-206624, AIAA-98-1018.
- [6] Reid MR, Scharfe DB, Webb RN. Computational evaluation of a latent heat energy storage system. *Sol Energy* 2013;95:99-105.
- [7] Kowalczyk W, Delgado A. Numerical simulation of phase change at high hydrostatic pressure under variable-gravity environment. *Numer Heat Transf Part A Appl* 2007;51:735-51.
- [8] Priebe J. The utilization of high output paraffin actuators in aerospace applications. In: 31th joint propulsion conference and exhibit. American Institute of Aeronautics and Astronautics; 1995. p. 1-7.
- [9] Mat S, Al-Abidi AA, Sopian K, Sulaiman MY, Mohammad AT. Enhance heat transfer for PCM melting in triplex tube with internal-external fins. *Energy Convers Manage* 2013;74:223-36.
- [10] Rabienataj Darzi AA, Jourabian M, Farhadi M. Melting and solidification of PCM enhanced by radial conductive fins and nanoparticles in cylindrical annulus. *Energy Convers Manage* 2016;118:253-63.
- [11] Bergles AE. Recent developments in enhanced heat transfer. *Heat Mass Transf* 2011;47(8):1001-08.
- [12] Jegadheeswaran S, Pohekar SD. Performance enhancement in latent heat thermal storage system: a review. *Renew Sustain Energy Rev* 2009;13:2225-44.
- [13] Mettawee ES, Assassa GMR. Thermal conductivity enhancement in a latent heat storage system. *Sol Energy* 2007;81:839-45.
- [14] Khodadadi JM, Hosseinzadeh SF. Nanoparticle-enhanced phase change materials (NEPCM) with great potential for improved thermal energy storage. *Int Commun Heat Mass Transfer* 2007;34:534-43.
- [15] Lacroix M, Benmadda M. Numerical simulation of natural convection-dominated melting and solidification from a finned vertical wall. *Numer Heat Transfer, Part A Appl* 1997;31:71-86.

- [16] Wang P, Yao H, Lan Z, Peng Z, Huang Y, Ding Y. Numerical investigation of PCM melting process in sleeve tube with internal fins. *Energy Convers Manage* 2016;110:428-35.
- [17] Ruan S, Zhang J, Cao J, Wang J, Xu T. Numerical Simulation of Melting Process of Phase Change Energy Storage Unit Under Microgravity. *J. Beijing Univ. Aeronaut. Astronaut.* 2018;44:2224-31.
- [18] Zhao CY, Lu W, Tian Y. Heat transfer enhancement for thermal energy storage using metal foams embedded within phase change materials (PCMs). *Solar Energy* 2010;84:1402-12.
- [19] Velraj R, Seeniraj RV, Hafner B, Faber C, Schwarzer K. Heat transfer enhancement in a latent heat storage system. *Solar Energy* 1999;65:171-80.
- [20] Sanusi O, Warzoha R, Fleischer AS. Energy storage and solidification of paraffin phase change material embedded with graphite nanofibers. *Int J Heat Mass Transfer* 2011;54:4429-36.
- [21] Nakhla D, Sadek H, Cotton JS. Melting performance enhancement in latent heat storage module using solid extraction electrohydrodynamics (EHD). *Int J Heat Mass Transf* 2015;81:695-704.
- [22] Seyed-Yagoobi J, Bryan JE. Enhancement of heat transfer and mass transport in single-phase and two-phase flows with electrohydrodynamics. *Adv. Heat Transf.* 1999;33:95-186.
- [23] Gao M, Cheng P, Quan X. An experimental investigation on effects of an electric field on bubble growth on a small heater in pool boiling. *Int J Heat Mass Transf* 2013;67:987-91.
- [24] Sadek H, Ching CY, Cotton J. The effect of pulsed electric fields on horizontal tube side convective condensation. *Int. J. Heat Mass Transfer* 2010;53:3721-32.
- [25] Heidarinejad G, Babaei R. Numerical investigation of electrohydrodynamics (EHD) enhanced water evaporation using Large Eddy Simulation turbulent model. *J. Electrostat.* 2015;77:76-87.
- [26] Nakhla D, Cotton JS. Effect of electrohydrodynamic (EHD) forces on charging of a vertical latent heat thermal storage module filled with octadecane. *Int. J. Heat Mass Transfer.* 2021;167:120828.
- [27] Luo K, Pérez AT, Wu J, Yi HL, Tan HP. Efficient lattice Boltzmann method for electrohydrodynamic solid-liquid phase change. *Phys. Rev. E.* 2019;100:013306.
- [28] Selvakumar RD, Qiang L, Luo K, Traoré P, Wu J. Numerical modeling of solid-liquid phase change under the influence an external electric field. *Int. J. Heat Mass Transfer* 2021;136:103550.
- [29] Marco P. Di, Grassi W. Pool boiling in micro-gravity: old and recent results, *Multiphase Sci. Tech-nol* 2007;19:141-165.
- [30] Nakhla D, Thompson E, Lacroix B, Cotton J. Measurement of heat transfer enhancement in melting of n-Octadecane under gravitational and electrohydrodynamics (EHD) forces. *J. Electrostat.* 2018;92:31-37.
- [31] Huang R, Wu H, Cheng P. A new lattice Boltzmann model for solid-liquid phase change. *Int J Heat Mass Transf* 2013;59:295-301.
- [32] Li Q, Luo K, Kang Q, He Y, Chen Q, Liu Q. Lattice boltzmann methods for multi-phase flow and phase-change heat transfer. *Prog Energy Combust Sci* 2016;52:62-105.
- [33] Huo Y, Rao Z. Lattice Boltzmann investigation on phase change of nanoparticle-enhanced phase change material in a cavity with separate plate. *Energy Convers Manage* 2017;154:420-9.
- [34] Luo K, Wu J, Yi HL, Tan HP. Lattice Boltzmann model for Coulomb-driven flows in dielectric liquids. *Phys. Rev. E* 2016;93:023309.
- [35] Luo K, Wu J, Yi HL, Tan HP. Numerical investigation of heat transfer enhancement in electro-thermo-convection in a square enclosure with an inner circular cylinder. *Int J Heat Mass Transf* 2017;113:1070-85.
- [36] He K, Chai Z, Wang L, Ma B, Shi B. Numerical investigation of electro-thermo-convection with a solid-liquid interface via the lattice Boltzmann method. *Phys. Fluids* 2021;33:037128.
- [37] Wang L, Wei Z, Li T, Chai Z, Shi B. A lattice Boltzmann modelling of electrohydrodynamic conduction phenomenon in dielectric liquids. *Appl. Math. Model.* 2021;95:361-78.
- [38] Guo Z, Shi B, Wang N. Lattice BGK model for incompressible Navier-Stokes equation, *J. Comput. Phys.* 2000;165:288-306.
- [39] Qian YH, d'Humières D, Lallemand P. Lattice BGK models for Navier-Stokes equation. *Europhys. Lett.* 1992;17:479.

- [40] Guo Z, Zheng C, Shi B. Discrete lattice effects on the forcing term in the lattice Boltzmann method. *Phys. Rev.* 2002;65:046308.
- [41] Chai Z, Shi B. A novel lattice Boltzmann model for the Poisson equation, *Appl. Math. Model.* 2008;32:2050-58
- [42] Chakraborty S, Chatterjee D. An enthalpy-based hybrid lattice–Boltzmann method for modelling solid–liquid phase transition in the presence of convective transport. *J. Fluid Mech.* 2007;592:155-175.
- [43] Lu J, Lei H, Dai C. An optimal two-relaxation-time lattice Boltzmann equation for solid-liquid phase change: the elimination of unphysical numerical diffusion, *Int. J. Therm. Sci.* 2019;135:17-29.
- [44] Mencinger J. Numerical simulation of melting in two-dimensional cavity using adaptive grid. *J. Comput. Phys.* 2004;198:243-264.
- [45] Wu J, Vázquez PA, Traoré P, Pérez AT. Finite amplitude electroconvection induced by strong unipolar injection between two coaxial cylinders. *Phys. Fluids* 2014;26:124105.
- [46] Wu J, Traoré P, Zhang M, Pérez AT, Vázquez PA. Charge injection enhanced natural convection heat transfer in horizontal concentric annuli filled with a dielectric liquid, *Int. J. Heat Mass Transf.* 2016;92:139-148.
- [47] Dhaidan NS, Khodadadi JM, Al-Hattab TA, Al-Mashat SM. Experimental and numerical investigation of melting of NePCM inside an annular container under a constant heat flux including the effect of eccentricity. *Int J Heat Mass Transfer* 2013;67:455-68.
- [48] Zhou H, Wei L, Cai Q, Ren X, Bi C, Zhong D, Liu Y. Annulus eccentric analysis of the melting and solidification behavior in a horizontal tube-in-shell storage unit. *Appl. Therm. Eng.* 2021;190:116752.
- [49] Darzi AAR, Farhadi M, Sedighi K. Numerical study of melting inside concentric and eccentric horizontal annulus. *Appl. Math. Model.* 2012;9:4080-86.
- [50] Luo K, Yi HL, Tan HP, Wu J. A unified lattice Boltzmann method for electric field-space charge coupled problems in complex geometries and its applications to annular electroconvection. *IEEE Trans. Ind. Appl.* 2017;53:3995-4007.

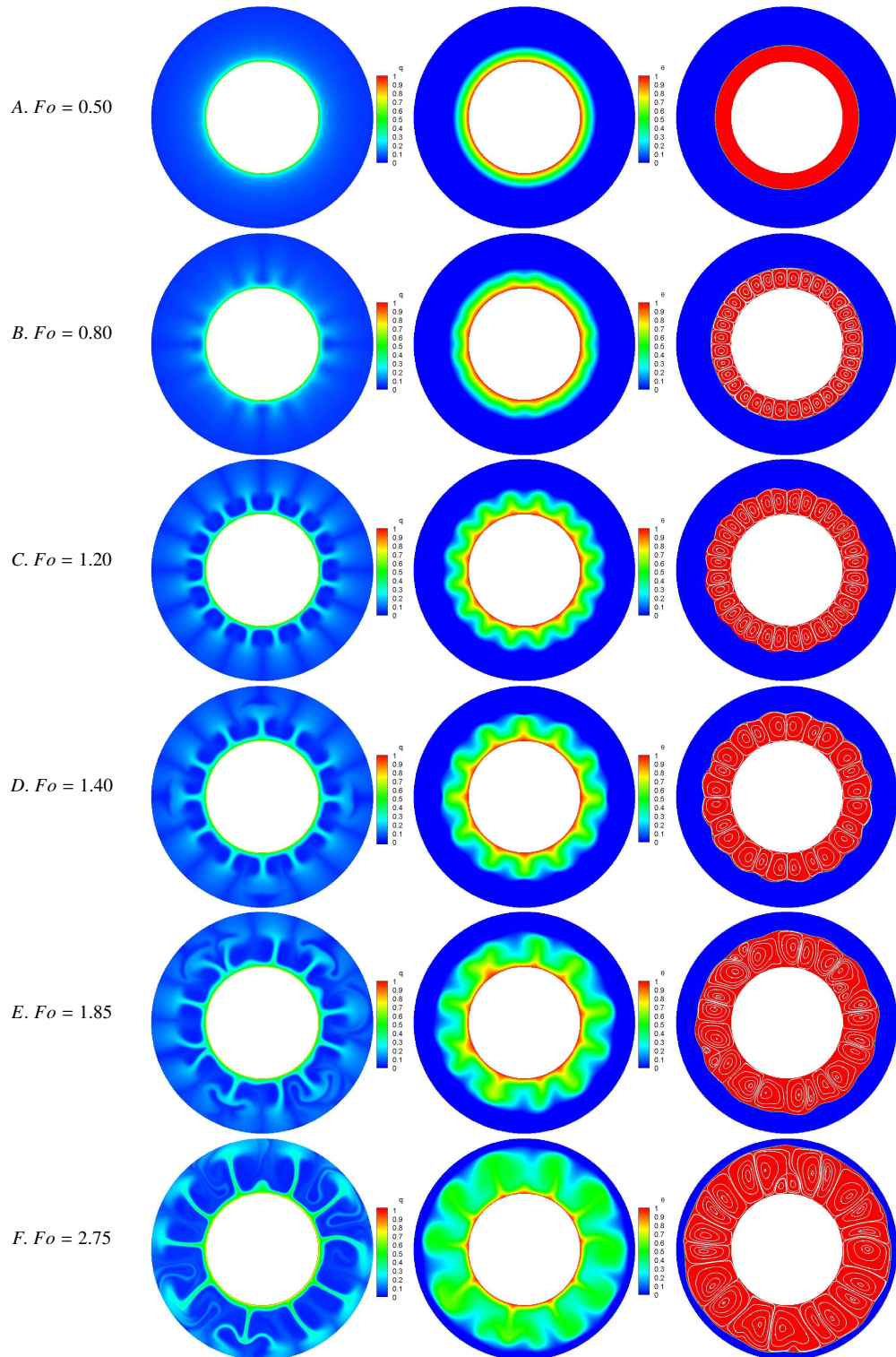


Figure 6: The transient distributions of charge density, temperature field and the liquid fraction with streamlines (from left to right) at six representative instants for $T = 1000$ under no-gravity condition.

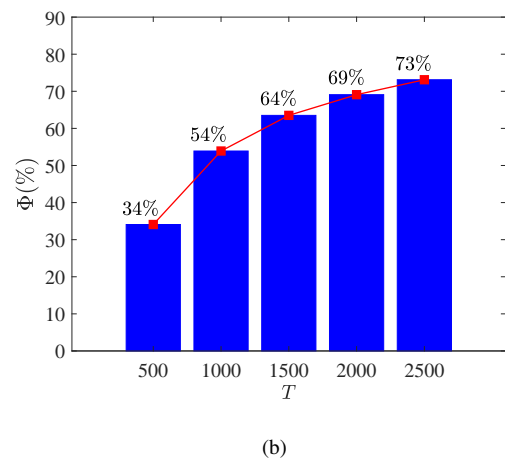
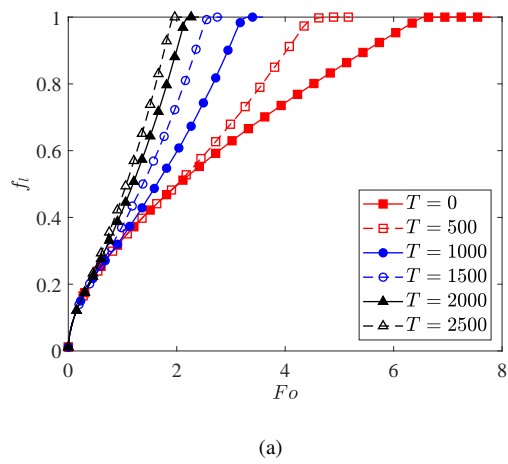


Figure 7: (a) Time evolution process of the total liquid fraction f_l , and (b) the percentages of charging time reduction for different electric Rayleigh number T under no-gravity condition.

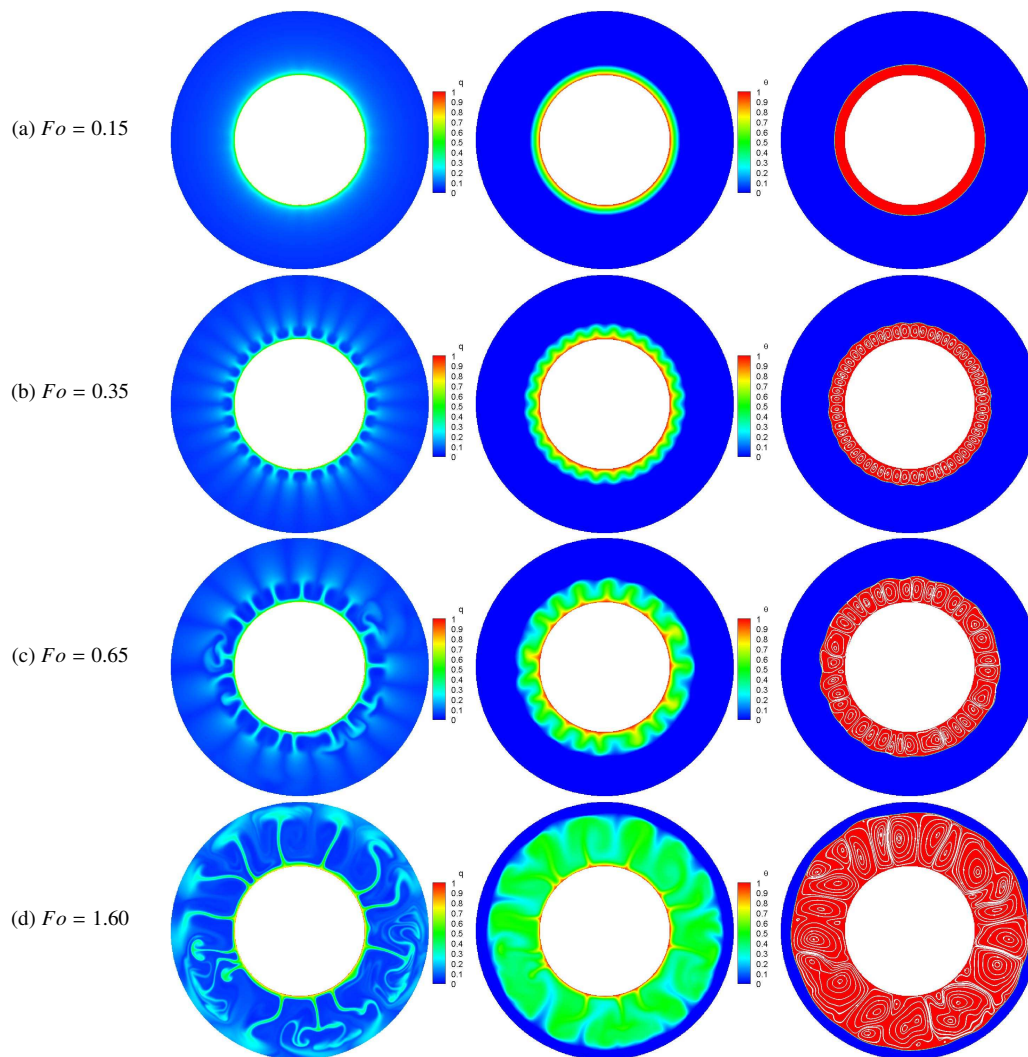


Figure 8: The transient distributions of charge density, temperature field and the liquid fraction with streamlines (from left to right) at four representative instants for $T = 2500$ under no-gravity condition.

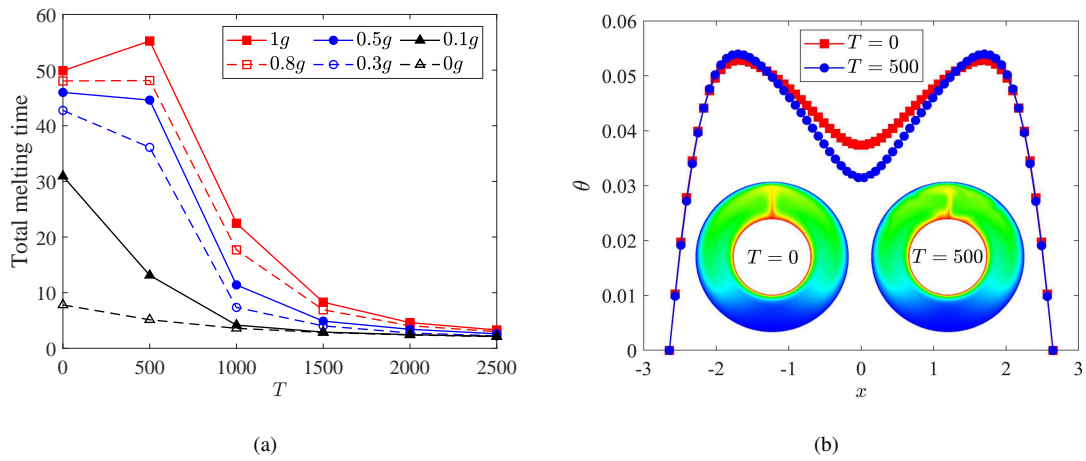


Figure 9: (a) Effects of the electric Rayleigh number on total melting time for different gravity conditions, and (b) isotherms for $T = 0$ (left) and $T = 500$ (right) at $Fo = 30$ with the corresponding temperature distributions along the horizontal central line of the lower half region.

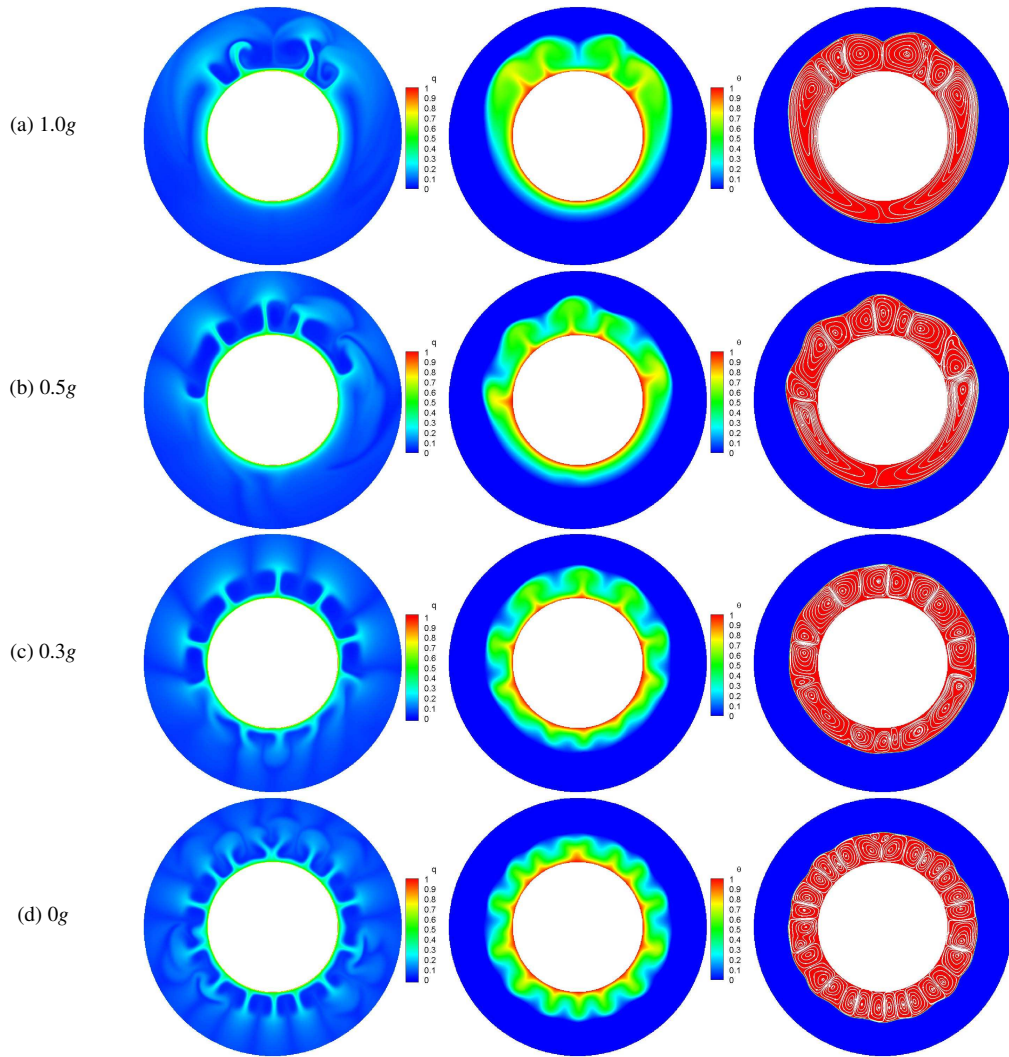
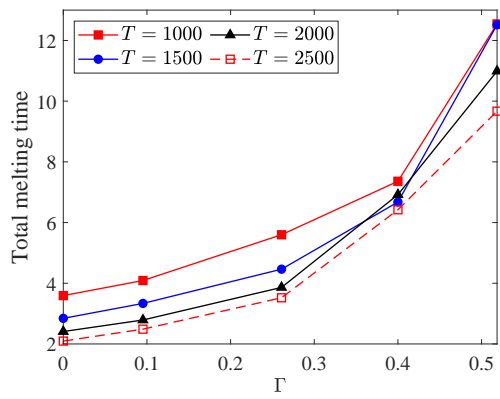
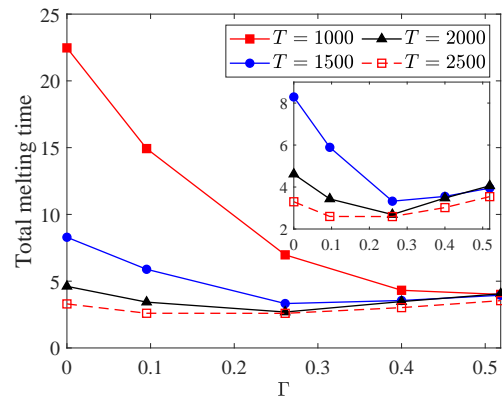


Figure 10: The transient distributions of charge density, temperature field and the liquid fraction with streamlines (from left to right) under different gravitational accelerations (a) 1.0g, (b) 0.5g, (c) 0.3g, (d) 0g at $Fo = 1.0$ with $T = 1500$.



(a)



(b)

Figure 11: Effects of the eccentricity on total melting time for different electric Rayleigh number under no-gravity (a) and normal gravity (b) conditions.

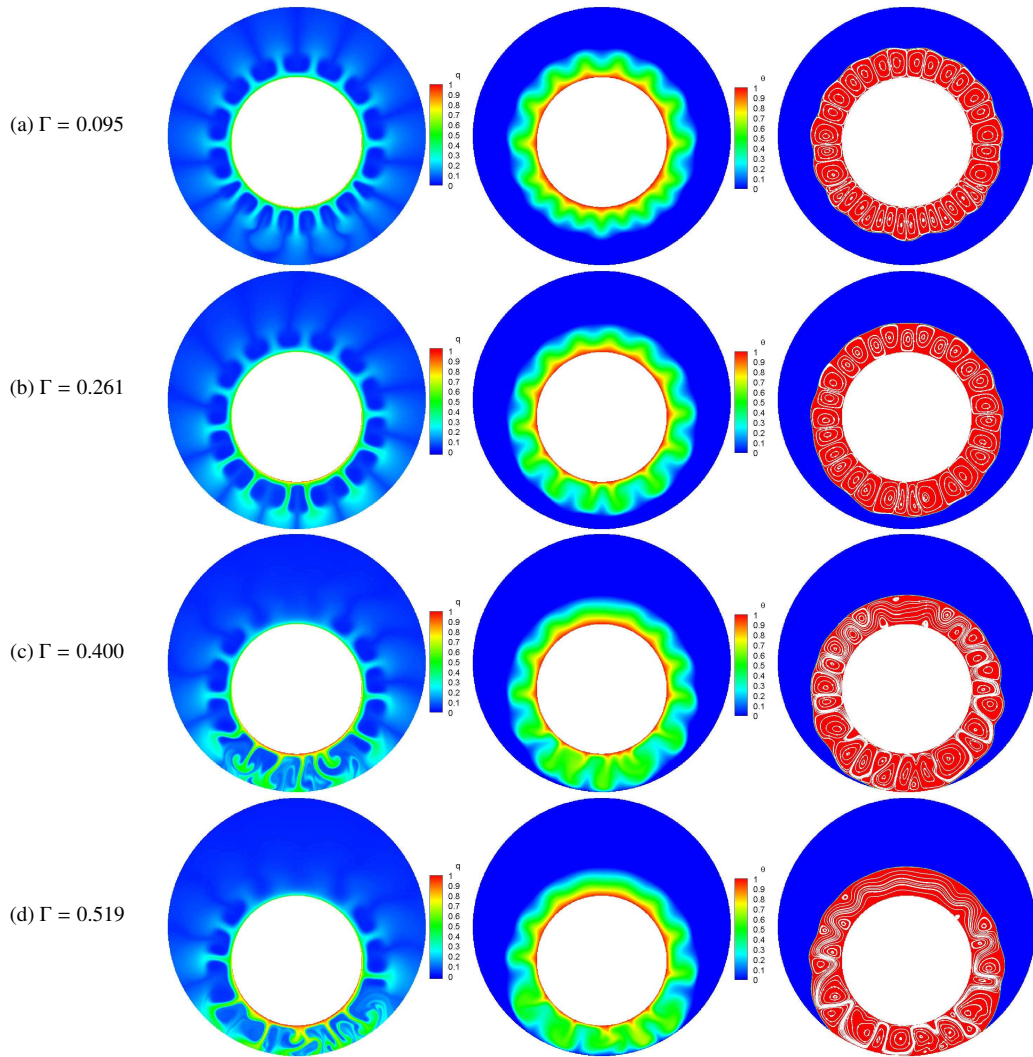


Figure 12: The transient distributions of charge density, temperature field and the liquid fraction with streamlines (from left to right) for (a) $\Gamma = 0.095$, (b) $\Gamma = 0.261$, (c) $\Gamma = 0.400$, (d) $\Gamma = 0.519$ at $Fo = 1.2$ with $T = 1000$ under no-gravity condition.